WILEY

Interrelations between dopamine and serotonin producing sites and regions of the default mode network

Feliberto de la Cruz[1] ⓘ | Gerd Wagner[2] | Andy Schumann[1] ⓘ | Stefanie Suttkus[1] |
Daniel Güllmar[3] | Jürgen R. Reichenbach[3] | Karl-Jürgen Bär[1] ⓘ

[1]Lab for Autonomic Neuroscience, Imaging and Cognition (LANIC), Department of Psychosomatic Medicine and Psychotherapy, Jena University Hospital, Germany

[2]Department of Psychiatry and Psychotherapy, Jena University Hospital, Germany

[3]Medical Physics Group, Department of Diagnostic and Interventional Radiology, Jena University Hospital, Germany

Correspondence
Karl-Jürgen Bär, Department of Psychosomatic Medicine and Psychotherapy, Jena University Hospital, Philosophenweg 3, 07743 Jena, Germany.
Email: karl-juergen.baer@med.uni-jena.de

Funding information
Universitätsklinikum Jena

Abstract

Recent functional magnetic resonance imaging (fMRI) studies showed that blood oxygenation level-dependent (BOLD) signal fluctuations in the default mode network (DMN) are functionally tightly connected to those in monoaminergic nuclei, producing dopamine (DA), and serotonin (5-HT) transmitters, in the midbrain/brainstem. We combined accelerated fMRI acquisition with spectral Granger causality and coherence analysis to investigate causal relationships between these areas. Both methods independently lead to similar results and confirm the existence of a top-down information flow in the resting-state condition, where activity in core DMN areas influences activity in the neuromodulatory centers producing DA/5-HT. We found that latencies range from milliseconds to seconds with high inter-subject variability, likely attributable to the resting condition. Our novel findings provide new insights into the functional organization of the human brain.

KEYWORDS

coherence, default mode network, dopamine, monoaminergic nuclei, serotonin, spectral Granger causality

1 | INTRODUCTION

Dopaminergic and serotonergic centers in the midbrain and brainstem are the primary sources of the neuromodulatory transmitters dopamine (DA) and serotonin (5-HT). They exert a profound influence on affective and cognitive processes in healthy subjects (Koot et al., 2012) and are considered to be functionally aberrant in various psychiatric disorders such as schizophrenia (Rolland et al., 2015) or major depression (Wagner et al., 2017).

Multiple lines of evidence suggest that blood oxygenation level-dependent (BOLD) signal fluctuations in the default mode network (DMN), are functionally tightly connected to these DA and 5-HT nuclei (Bär et al., 2016; Tomasi & Volkow, 2014; Wagner et al., 2018).

The DMN is one of the most widely studied functional brain networks. At rest, when the mind is engaged in preprocessing of one's own mental interior, the DMN exhibits increased activity and energy consumption while exhibiting lower activity during focusing on external stimuli (Greicius, Krasnow, Reiss, & Menon, 2003; Raichle et al., 2001). Core regions within the DMN are the ventromedial prefrontal cortex (VMPFC), the perigenual anterior cingulate cortex (pACC), the dorsomedial prefrontal cortex (DMPFC), the posterior cingulate cortex (PCC), the inferior parietal lobule, the lateral temporal cortex and the hippocampal formation (Buckner, Andrews-Hanna, & Schacter, 2008).

Pharmacological studies have demonstrated that activity within the DMN is influenced by DA and 5-HT neurotransmission (Carhart-Harris et al., 2013; Kelly et al., 2009; Kunisato et al., 2011; Metzger, Wiegers, Walter, Abler, & Graf, 2016; Nagano-Saito et al., 2008;

van de Ven, Wingen, Kuypers, Ramaekers, & Formisano, 2013; van Wingen et al., 2014; Wagner et al., 2017). For instance, the fractional amplitude of low-frequency fluctuations in DMN areas is altered during acute tryptophan depletion (ATD), a technique used to decrease plasma levels of the 5-HT precursor tryptophan (Bär et al., 2020; Kunisato et al., 2011). Similarly, the functional connectivity between frontal areas and striatum is reduced under conditions of DA depletion (Nagano-Saito et al., 2008). In a more recent study, van Wingen and colleagues reported reduced functional connectivity between VMPFC and lateral parietal cortex after prolonged intake of serotonin-norepinephrine reuptake inhibitors (van Wingen et al., 2014). Together, these studies demonstrate that the functional integrity of the DMN is subject to the influence of the neurotransmitters 5-HT and DA.

Anatomically, the ascending monoamine systems are widely distributed across multiple brain regions, including core areas of the DMN. The ventral tegmental area (VTA) and substantia nigra pars compacta (SNc)—the DA-synthesizing centers—are the respective origins of the mesocorticolimbic dopaminergic and nigrostriatal systems (Ungerstedt, 1971). The mesocorticolimbic dopaminergic system projects from VTA to the nucleus accumbens (Nac) and cortical and limbic regions, including the medial prefrontal cortex, hippocampus, and amygdala (Ikemoto, 2007). Similarly, the 5-HT system projects from the two upper raphe nuclei—the nucleus raphes dorsalis (DRN) and nucleus centralis superior (NCS)—via the thalamus to the amygdala and hippocampus and reaches distant regions such as VMPFC and PCC (Azmitia & Segal, 1978).

Recently, using resting-state functional connectivity and graph theoretical analysis, we found that BOLD signal fluctuations in DA and 5-HT centers were significantly correlated with signal fluctuations in VMPFC and PCC and that those centers were thus functionally integrated into the DMN (Bär et al., 2016). Although this study showed the existence of a functional interplay between dopaminergic/serotonergic nuclei and the DMN, there is still little understanding of the directional causal relationship between these regions.

Causal relationships or effective connectivity measures the direct influence that a given neuronal system exerts over others (Friston, 1994), thus providing a mechanistic model to explain the cause of specific functional interactions between brain regions. Combining methods to assess effective connectivity, for example, Granger causality (GC) (Abler et al., 2006; Deshpande, LaConte, James, Peltier, & Hu, 2009; Gaglianese, Costagli, Bernardi, Ricciardi, & Pietrini, 2012; Kayser, Sun, & D'Esposito, 2009; Roebroeck, Formisano, & Goebel, 2005; Seth, Chorley, & Barnett, 2013; Stenner et al., 2015) and methods that quantify the relative latencies between connected areas, such as coherence-based phase delay (Biswal, Yetkin, Haughton, & Hyde, 1995; Lauritzen, D'Esposito, Heeger, & Silver, 2009; Sun, Miller, & D'Esposito, 2005), might improve the understanding of the temporal hierarchy between regions. GC is a data-driven exploratory approach based on linear regressive models that can be applied directly to any time series and does not require prior assumptions about the underlying neural circuitry (Roebroeck, Formisano, & Goebel, 2011). While this method allows inferences about effective connectivity based on the temporal precedence between time-series,

it cannot directly measure the relative timing between them. Measuring temporal delays in the brain is crucial to assess how the network's regions interact and to unravel the sequence of cognitive processes within the network (Sun et al., 2005). Coherence-based methods can estimate time delays by determining phase differences in the coherence between fMRI time series (Lauritzen et al., 2009; Sun et al., 2005). Since the calculation of coherence-based phase delays takes place in the frequency domain, it is largely unaffected by regional variations in the shape of the hemodynamic response function (HRF) (Aguirre, Zarahn, & D'Esposito, 1998; Handwerker, Ollinger, & D'Esposito, 2004). The combination of GC and coherence-based methods has been used in the past to investigate the functional organization of the motor cortex (Brovelli et al., 2004; Kayser et al., 2009) and visual areas (Gaglianese et al., 2012).

Despite the advantages that both methods offer over other approaches, their application to fMRI data can be compromised by several factors. In particular, the temporal scale on which the data is sampled is critical for the interpretation of GC and coherence. Standard fMRI protocols involve sampling intervals (TR) of a few seconds, which by far exceed the millisecond scale of typical inter-neuron delays. Using long TR can lead to pseudocausality impacting the model order estimation in GC (Kayser et al., 2009; Seth et al., 2013). Similarly, the phase-delay fails to capture the corresponding latency between two time-series if the TR becomes too long (Kayser et al., 2009). Recent progress in simultaneous multi-slice acquisition using parallel imaging has made it possible to reduce TR by more than 10 times (Feinberg et al., 2010). At this fine-grained temporal scale, the sensitivity and stability of GC are increased compared with standard acquisitions (Lin et al., 2014; Wen, Rangarajan, & Ding, 2013).

The present study aims to gain more insight into the causal relationship between DMN regions and the DA and 5-HT nuclei. Based on the pharmacological (Kunisato et al., 2011; Nagano-Saito et al., 2008; van Wingen et al., 2014) and known anatomical (Azmitia & Segal, 1978; Ikemoto, 2007) evidences linking DA and 5-HT centers located in midbrain/brainstem with DMN, we tested the hypothesis that these neuromodulatory centers exert a primary bottom-up drive to DMN. To this end, we estimated interregional interactions during the resting-state condition by describing the temporal relationship between BOLD signal fluctuations in core DMN regions and midbrain/brainstem nuclei using Granger causality and phase delay analysis. To overcome the above-mentioned methodological concerns regarding the slow temporal fMRI resolution, we used an ultra-fast fMRI acquisition while preserving a relatively high spatial resolution.

2 | MATERIAL AND METHODS

2.1 | Subjects

Thirty-two healthy subjects (average age = 24.9 ± 2.5 years, range: 21–31 years, 18 females) recruited from the local university community were studied using resting-state fMRI. None of the participants had any present or past history of psychiatric, neurological, or other

clinically significant disorders, as assessed by the short form of the structured diagnostic interview for ICD-10 psychiatric disorders (M.I. N.I. International Neuropsychiatric Interview (Sheehan et al., 1998). According to the modified version of the Annett's handedness inventory (Briggs & Nebes, 1975), all participants were right-handed. Informed written consent was obtained in accordance with the protocols approved by the local Ethics Committee.

2.2 | Data acquisition

Data were collected on a 3T whole body-system equipped with a 12-element head matrix coil (MAGNETOM TIM Trio, Siemens). The protocol consisted of a resting state scan followed by a structural scan. Participants were instructed to keep their eyes closed during the entire measurement. T_2^*-weighted images were obtained using a multiband multislice GE-EPI sequence (TR = 484 ms, TE =30 ms, flip angle = 90°, multiband factor = 8) with 56 contiguous transverse slices of 2.5 mm thickness covering the entire brain and including the lower brainstem. The matrix size was 78 × 78 pixels with an in-plane resolution of (2.5 × 2.5) mm^2 corresponding to a field of view of 195 mm × 195 mm. A series of 1900 whole-brain volume sets were acquired in one session lasting ~15 min. The choice of fMRI parameters represents a trade-off between fMRI imaging of the cortex and midbrain/brainstem and reliable estimation of GC and phase-delay. Given the susceptibility of midbrain/brainstem areas to signal loss and image distortion, fMRI data were visually inspected for these artifacts. None of the participants' data had to be discarded due to excessive signal loss or distortion.

High-resolution anatomical T_1-weighted volume scans (MP-RAGE) were obtained in sagittal orientation (TR = 2,300 ms, TE = 3.03 ms, TI = 900 ms, flip angle = 9°), FOV = 256 mm × 256 mm, matrix 256 × 256, number of sagittal slices = 192, acceleration factor (PAT = 2) with an isotropic resolution of (1 × 1 × 1) mm^3.

2.3 | Physiological recordings during fMRI

During the fMRI scan, respiratory and cardiac signals were recorded simultaneously using an MR-compatible BIOPAC MP150 polygraph (BIOPAC Systems Inc., Goleta, CA) and digitized at 500 Hz. Respiratory activity was assessed by a strain gauge transducer incorporated in a belt tied around the chest, approximately at the level of the processus xiphoideus. The cardiac signal, photoplethysmograph (PPG) signal, was recorded using a pulse oximeter attached to the proximal phalanx of the index finger of the subject's left hand.

To remove MRI-related or movement artifacts, the PPG signal was band-pass filtered (0.05–3 Hz), and the respiratory signal was low-pass filtered with a cutoff frequency of 10 Hz. Pulse-wave onsets were automatically extracted by detecting peaks of the temporal derivative of the filtered PPG signal (Schumann et al., 2018). The quality of peak detection was visually inspected. Correction of false positives (related to movements or extrasystolic beats) was performed by

seeking the true pulse wave, while negatives (lack of detection) were approximated by taking half of the interval between the two adjacent beats.

2.4 | fMRI preprocessing

Resting-state data analysis was performed using SPM12 (http://www.fil.ion.ucl.ac.uk/spm) and AFNI software package (https://afni.nimh.nih.gov/). The first 20 images were discarded to ensure a steady-state tissue magnetization condition. Physiological noise correction was conducted by regressing eight RETROICOR regressors on a slice-wise basis to model the effects of the respiratory and cardiac cycles (Glover, Li, & Ress, 2000). We also generated five regressors for respiration volumes per time (RVT) on a slice-wise basis, which model slow blood oxygenation level fluctuations (Birn, Smith, Jones, & Bandettini, 2008). The RVT regressors consisted of the RVT function and four delayed terms at 5, 10, 15, and 20 s, respectively (Birn et al., 2008). By combining the RETROICOR with the RVT regressors, the BOLD signal was cleaned from almost all physiologically-induced fluctuations. RETROICOR and RVT regressors were generated by AFNI's "RetroTS.m," which takes the cardiac and respiratory time series, synchronized with the fMRI acquisition, as input (Jo, Saad, Simmons, Milbury, & Cox, 2010).

Further preprocessing steps of the fMRI data included rigid body realignment to the mean of all images, removal of motion parameters using multiple regression, and high pass filtering to remove all non-relevant ultra-slow fluctuations below 0.01 Hz. Since GC analysis of BOLD time-series relies on high-frequency deflection due to the low-order autoregressive model, no low-pass filtering was performed. For resting-state functional connectivity analysis (RSFC), data were further low-pass filtered with a cutoff frequency of 0.08 Hz along with regression of white matter and cerebrospinal fluid signals and smoothed with a 6 mm full-width-at-half-maximum Gaussian kernel. Finally, images were normalized to the MNI space using the DARTEL (diffeomorphic anatomical registration through exponentiated Lie algebra) procedure integrated into SPM12 (Ashburner, 2007).

To improve the normalization procedure and to more precisely define regions-of-interest (ROIs) within the midbrain and brainstem for the subsequent time-series extraction, neuroimaging data were normalized to the spatially unbiased infra-tentorial template (SUIT, version 3.1) (Diedrichsen, 2006), available as an open-source SPM-toolbox. This procedure was performed after following all previous steps up to high-pass filtering with the cutoff frequency of 0.01 Hz. Using the SUIT toolbox, we applied the following preprocessing steps: (a) segmentation of the whole-brain image dataset as implemented in SPM12, (b) cropping of the image dataset, retaining only the cerebellum and brainstem, (c) normalization using the DARTEL engine (Ashburner, 2007), which uses gray- and white-matter segmentation maps produced during cerebellar isolation to generate a flowfield using Large Deformation Diffeomorphic Metric Mapping (LDDMM, Beg, Miller, Trouvé, & Younes, 2005), and (d) reslicing to a voxel size of (2 × 2 × 2) mm^3.

2.5 | Definition of the seed regions

We focused on two dopaminergic centers located in the midbrain and two serotonergic centers in the brainstem. The dopamine-producing ventral tegmental area (VTA, A10) and substantia nigra pars compacta (SNc, A9) (Dahlström & Fuxe, 1964) and the two upper serotonergic Raphe nuclei, raphe dorsalis (DRN, B7) and nucleus centralis superior (NCS, B6 + B8), have been shown to be functionally connected and integrated into the DMN (Bär et al., 2016).

The definition of the location of the VTA and SNc was based on available atlases of the human brainstem (Naidich et al., 2009; Paxinos & Huang, 1995). Due to the high concentration of neuromelanin, the SNc (pars compacta) has a marked contrast to the SN pars reticulata (Yelnik, François, Percheron, & Heyner, 1987) and can be discriminated from neighboring regions, including the red nucleus and the superior cerebellar peduncle, to which it is located dorsolaterally. The VTA was defined by its lateral boundary adjacent to the substantia nigra, medial boundary adjacent to the inter-peduncular fossa, and its extent in the posterior direction to halfway up the medial edge of the red nucleus. Finally, VTA and SNc nuclei were merged to form a single dopaminergic ROI (DOP). The DRN (MNI-coordinates, x = 2, y = −26, z = −18) and NCS (MNI-coordinates, x = 0, y = −32, z = −24) nuclei were defined as spherical ROIs of 4 mm radius and also merged to form a serotonergic ROI (SER). Other ROIs included the two core regions of the DMN, that is, PCC (MNI-coordinates, x = −4, y = −56, z = 22) and VMPFC (MNI-coordinates, x = 0, y = 44, z = −14), and the thalamus (MNI-coordinates, x = 1, y = −12, z = 10). We included the thalamus because all ascending DA and 5-HT projections to subcortical and cortical regions pass through it. It serves as a functional and anatomical hub (Hwang, Hallquist, & Luna, 2013; Sherman, 2007) and has strong functional connectivity with midbrain/brainstem and DMN regions (Bär et al., 2016). The VMPFC and PCC ROIs were drawn as spheres of 10 mm radius, as defined in our previous studies (de la Cruz et al., 2019; de la Cruz, Schumann, Köhler, Bär, & Wagner, 2017), while the thalamic ROI was created using the WFU Pick Atlas (Maldjian, Laurienti, & Burdette, 2004; Maldjian, Laurienti, Kraft, & Burdette, 2003). Figure 1 shows all ROIs used throughout the study.

2.6 | Spectral Granger causality

Granger causality relies on the assumption that given two jointly distributed stochastic processes, say X and Y, the prediction of the variable X can be improved by incorporating past values of Y (Granger, 1969). Each variable, X and Y, can be modeled as an autoregressive (AR) process of order p. Here, we used spectral Granger causality (SGC) to examine the direction of influence between DMN areas and DA/5-HT nuclei in the resting state frequency range (i.e., 0.01–0.08; RS-band). SCG has the advantage of having a frequency domain decomposition, and in doing so, one may find at which frequencies two variables interact with each other. The causal spectral influence from Y to X at frequency λ can be defined as (Barnett & Seth, 2011):
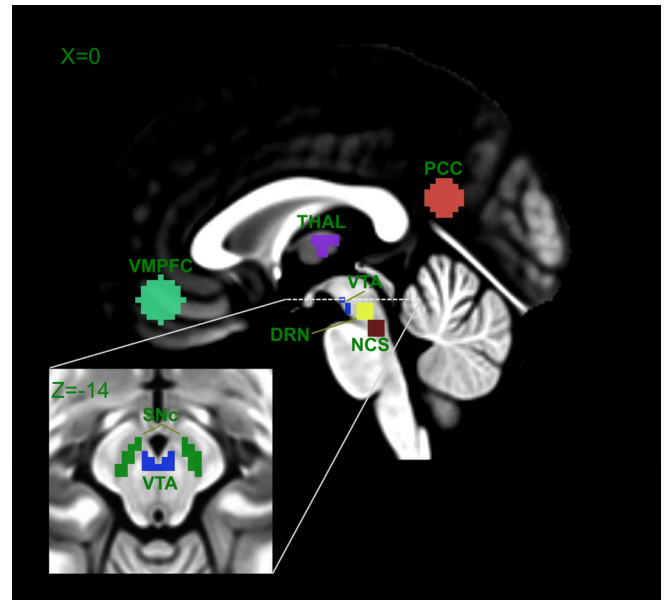

FIGURE 1 Anatomical location of ventromedial prefrontal cortex (VMPFC), thalamus (THAL), posterior cingulate cortex (PCC), ventral tegmental area (VTA), substantia nigra (SNc), dorsal raphe nucleus (DRN), and nucleus centralis superior (NCS). VTA and SNc were merged into a single DOP ROI and DRN and NCS into a single SER ROI

$$f_{y \to x}(\lambda) = \ln \frac{|S_{xx}(\lambda)|}{\left| S_{xx}(\lambda) - H_{xy}(\lambda) \Sigma_{y/x} H^*_{xy}(\lambda) \right|}$$

In the above equation, $S_{xx}(\lambda)$ is the auto-spectrum of X, $H_{xy}(\lambda)$ and its complex conjugate $H^*_{xy}(\lambda)$ represent the transfer function and are related to the inverse Fourier Transform of the model coefficients. $\Sigma_{y|x}$ is defined as: $\Sigma_{yy} - \Sigma_{yx}\Sigma_{xx}^{-1}\Sigma_{xy}$, where Σ_{yy}, Σ_{xx} and Σ_{yx}, Σ_{xy} are the diagonal and off-diagonal elements of the covariance matrix of residuals, respectively.

If we are only interested in a specific frequency range, for example, resting-state frequency range, then the SGC value can be obtained by integrating over this frequency range:

$F_{y \to x} = \frac{1}{f_2 - f_1} \int_{f1}^{f2} f_{y \to x}(\lambda) d\lambda$ where f_1 and f_2 correspond to 0.01 and 0.08 Hz, respectively.

For each pair of ROIs, optimal orders of the autoregressive model were derived using the Bayesian information criterion (BIC; [Schwarz, 1978]). The derived model orders ranged between 0 and 6, with a mean value of 3. An additional test with a fixed model order of 3 was performed, but no appreciable differences were noticed.

2.7 | Phase delay analysis

The phase-delay analysis was performed by using the same ROIs as for SGC. We used Welch's modified periodogram averaging method to estimate power-spectral and cross-spectral density (Welch, 1967). Welch's method offers high spectral resolution and provides a better noise reduction than the conventional Fourier transform. It splits the

fMRI time series into overlapping segments, which are then windowed in order to reduce spectral leakage. The noise reduction is accomplished by averaging the cross-spectrum over all previously windowed segments. Here, we used a 256-point discrete Fourier transform, a Hanning window, and an overlap of 126 points to compute the periodogram. The phase-delay was estimated by calculating the average slope of the phase-spectrum, which can be written: $\tau = -\varphi(\lambda)/(2\pi\lambda)$, where $\varphi(\lambda)$ is the phase-spectrum at the respective frequency λ (Sun et al., 2005). Finally, the phase-delay was averaged over the RS-band. The analysis was conducted using the Python library nitime (nipy.org/nitime).

2.8 | Statistical analysis

Group-level RSFC maps for DOP and SER ROIs were computed using a one-sample t test. To correct these maps for multiple comparisons, we performed a spatial clustering operation using the AFNI's *ClustSim* function with 10,000 Monte Carlo simulations. This procedure allowed us to set a corrected $p < .05$ for a minimum cluster size of 209 voxels at an initial threshold of $p < .001$.

We employed nonparametric permutation testing to assess the statistical significance of SCG (Brovelli et al., 2004). The permutation test was conducted as follows: subject's time series were randomly shuffled 1,000 times to derive an empirical null distribution of SGC values at each frequency. For each frequency bin, a p-value was computed as the proportion of permutations that resulted in an SGC value greater than that obtained from the original data. These p-values were corrected for multiple comparisons across frequency bins using FDR correction, and those less than 5% were considered statistically significant. Finally, we computed the percentage of subjects where SGC was statistically significant.

For statistical analysis of phase-delay, a similar approach was performed using a two-sided one-sample permutation test. Here, the sign of the sample's phase-delay values is collected and randomly assigned (1,000 times) to the absolute values of the sample to derive an empirical null distribution of mean values. The significance level (p-value) is found by estimating the proportion of values greater than the mean of the original data. p-values less than 5% were considered statistically significant.

3 | RESULTS

3.1 | Resting state functional connectivity

We conducted a whole-brain correlation analysis using both DOP and SER ROIs as seed regions. Voxels significantly positively correlated with DOP ROI were found in the anterior cingulate cortex (ACC), mid-cingulate cortex (MCC), VMPFC, precuneus/PCC, thalamus, brainstem (medulla) and cerebellum (Figure 2, top). Most of these regions are part of the DMN. Significantly negatively correlated voxels with DOP ROI were observed in the left and right occipital cortices.

With respect to the SER ROI, the clusters that survived the statistical threshold exhibited a lower number of significant voxels compared to the DOP ROI (Figure 2, bottom). We found voxels positively correlated with SER ROI in ACC, VMPFC, precuneus/PCC, thalamus, and cerebellum, while those with negative correlations were observed in the left and right occipital cortices. Table 1 summarizes the clusters with significant RSFC for both seed regions.

3.2 | SGC

SGC results are depicted in Table 2. The dominant SGC direction is highlighted in bold, while values in parentheses indicate the percentage of subjects with significant ($p < .05$, FDR-corrected) SGC in the resting-state frequency range. Overall, the SGC values were stronger
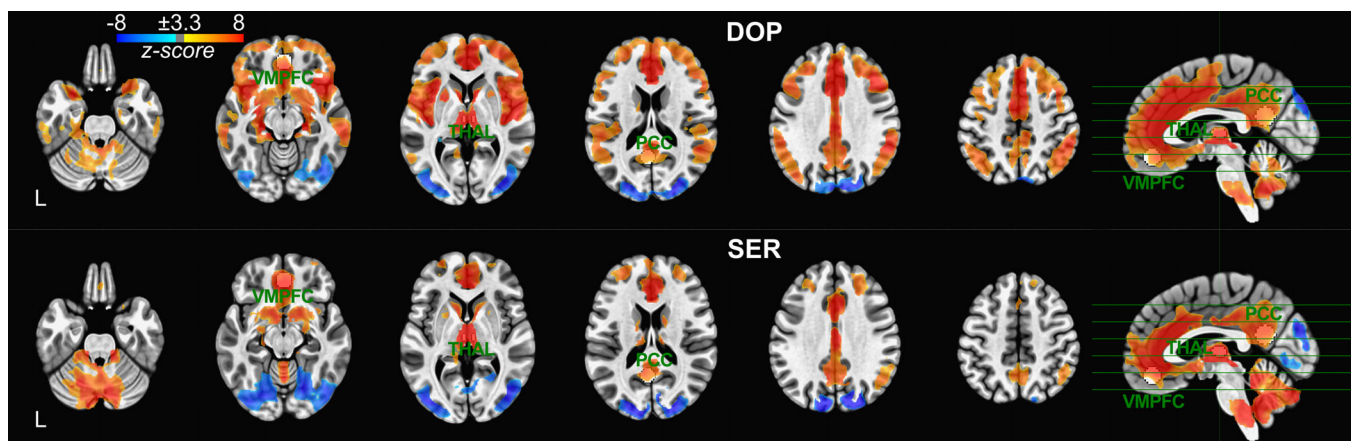

FIGURE 2 Functional connectivity maps of dopaminergic (DOP) and serotonergic (SER) seed regions (one-sample t test at voxel-level $p < .001$ and at cluster-level $p < .05$ FWE-corrected corresponding to a minimum cluster size of 209 voxels using AFNI's ClustSim). The z-score maps have been masked to exclude areas outside the brain and to avoid autocorrelation. VMPFC, PCC, and thalamic ROIs are overlaid on functional connectivity maps for illustration

TABLE 1 Brain areas showing significant functional connectivity with the dopaminergic and serotonergic ROIs

Functional connectivity	Left/right	Brodmann's area	Cluster size	MNI coordinate			Z-score*
				x	y	z	
Seed: Dopaminergic ROI							
Anterior cingulate cortex		24	80,067	−6	24	22	7,44
Ventromedial prefontal cortex		10/11		6	30	−12	6,59
Insula	L/R	13		−42	14	0	6,82
Thalamus	L/R			−14	−4	10	6,83
Parahippocampal gyrus	L/R			24	−26	−10	6,13
Caudate	L			−10	6	4	7,04
Dorsolateral prefrontal cortex	L/R	8/9		46	28	22	5,27
Superior temporal gyrus	L/R			50	−22	8	5,97
Posterior cingulate cortex		23/31		6	−44	22	6,61
Precuneus	L/R	39		−42	−76	34	6,12
Inferior parietal cortex	L/R	40		58	−46	40	6,61
Supplementary motor area	L	6		−40	8	40	5,73
Brainstem				−3	−34	−51	4,82
Cerebellum	L/R			−10	−60	−42	7,17
Occipital cortex	L/R	19	12,256	42	−80	0	−7,15
Seed: serotonergic ROI							
Anterior cingulate cortex		22	37,954	−2	30	24	5,93
Ventromedial prefontal cortex		10/11		−8	46	−8	5,93
Thalamus	L/R			11	−13	4	7,89
Caudate	L/R			10	14	−4	6,63
Posterior cingulate cortex		23/31		−10	−58	28	6,11
Precuneus		31		12	−62	34	5,64
Brainstem				3	−35	−40	4,95
Cerebellum	L/R			1	−61	−37	6,72
Dorsolateral prefrontal cortex	R	9	1,204	28	40	38	6,01
Occipital cortex	L/R	19	11,235	44	−72	−8	−6,19

Note: Statistical significance level set at $p < .05$ FWE-corrected (with a combined voxel-level threshold at $p < .001$ and a minimum cluster size of 209 voxels using AFNI' ClustSim).

	Target				
Source		PCC	VMPFC	THAL	DOP	SER
	PCC		**0.188** (100%)	**0.079** (84%)	**0.039** (75%)	**0.031** (66%)
	VMPFC	0.088 (94%)		**0.049** (69%)	**0.027** (56%)	0.027 (66%)
	THAL	0.035 (56%)	0.034 (63%)		**0.040** (72%)	**0.033** (56%)
	DOP	0.007 (28%)	0.009 (34%)	0.022 (66%)		**0.005** (28%)
	SER	0.007 (28%)	0.006 (31%)	0.008 (38%)	0.002 (25%)	

TABLE 2 The table values are group mean Granger causality with prediction going from source (row) to target (column)

Note: The dominant direction is highlighted in bold. Values within parentheses represent the percent of subjects with significant ($p < .05$ FDR corrected) Granger causality.
Abbreviations: DOP, dopaminergic area; PCC, posterior cingulate cortex; SER, serotonergic area; THAL, thalamus; VMPFC, ventromedial prefrontal cortex.

in the descending direction than in the ascending direction, suggesting that DMN areas better predict BOLD signal fluctuations in the DOP/SER than vice versa. For instance, the SGC value was five times higher in the direction from PCC to DOP than in the opposite direction. Similarly, the SGC value from VMPFC to SER is more than four times higher than that from SER to VMPFC.
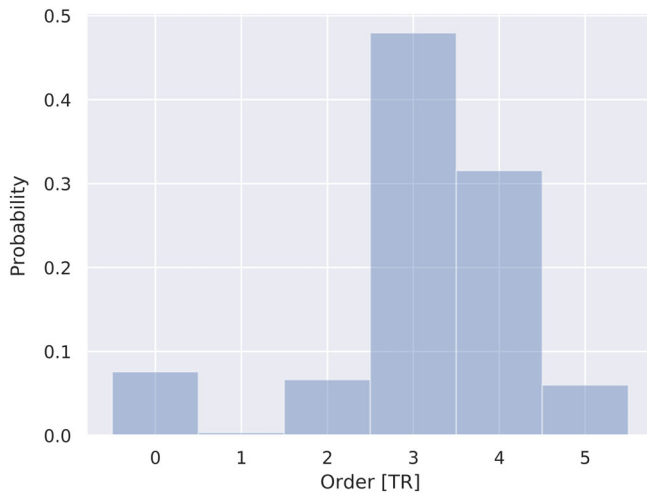
FIGURE 3 Distribution of optimal order-lags for all pairs of ROI comparisons in all subjects

FIGURE 4 Phase-delay information flow. The arrow indicates the lagged region. The number represents the averaged relative latency in seconds between the two corresponding regions, whereas the value in parentheses their respective standard deviation. *$p < .05$ based on the permutation test. Abbreviations: VMPFC, ventromedial prefrontal cortex; PCC, posterior cingulate cortex; DOP, dopaminergic area; SER, serotonergic area; THAL, thalamus

Furthermore, 72% of subjects exhibited significant SGC values from the thalamus to DOP, while in 56% of them, the SGC values were significant from the thalamus to SER. The information flow in the opposite direction was significant in 66 and 38% of subjects from DOP and SER to the thalamus, respectively. Interestingly, despite their spatial proximity, less than 29% of subjects showed significant SGC values between DOP and SER nuclei in both directions. For both DMN ROIs, the more substantial influence was found from PCC to VMPFC. Here, significant SGC values were found in 100 and 94% of subjects from PCC to VMPFC and VMPFC to PCC, respectively.

As shown in Figure 3, the optimal order-lags of the autoregressive model for all subjects and ROIs combination as estimated by BIC varied from 0 to 6 and has the highest probability at 3 (~1.5 s). This mean order-lag of 1.5 s is in correspondence with the latencies measured by the coherence analysis (see phase delay section) and with the results of previous studies using Granger causality (Gaglianese et al., 2012; Kayser et al., 2009).

3.3 | Phase delay

The relative BOLD latencies between the brainstem/midbrain nuclei, thalamus, and DMN areas using phase delay analysis are illustrated in Figure 4. Except for the pair THAL-DOP, the phase delay map mainly corresponds with GC results. The average phase delay characterizing the connection PCC-DOP was 1.41 ± 1.72 s, which means that activity in DOP follows activity in PCC by almost 2 s. The same behavior was found between VMPFC and DOP, where activity in DOP followed that in VMPFC by 1 s (0.91 ± 2.06 s). Despite the large standard deviations, phase delay values characterizing the connection DMN-DOP were significant ($p < .05$), as determined by a permutation test ($p < .05$). None of the average phase delay values between DMN regions and SER was significant.
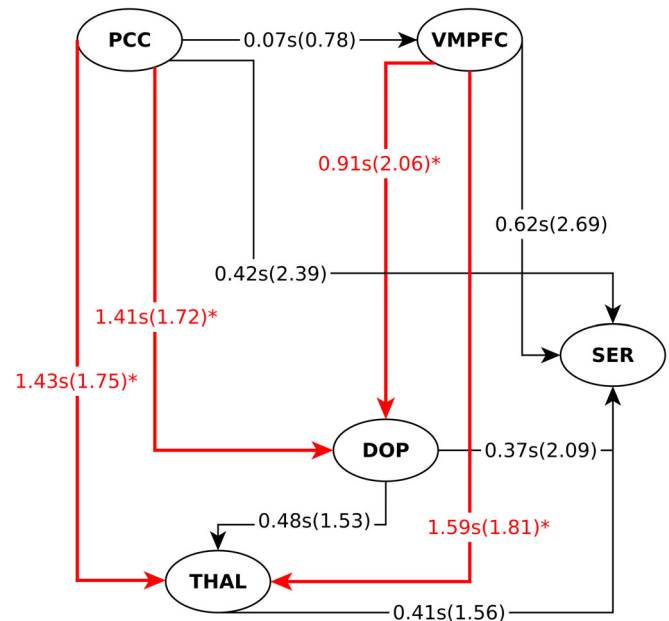
Interestingly, the largest and most significant latencies, relative to all other ROIs, were observed between DMN nuclei and the thalamus.

In Figure 5, the SGC and phase delay results are combined. The combination of both findings suggests that activation in the core DMN regions precede those from the dopaminergic and serotonergic nuclei. Thus, in contrast to the hypothesis that brainstem/midbrain monoaminergic centers provide bottom-up modulatory influence on the DMN, the phase delay and SGC results suggest that in the resting-state condition, both core DMN regions, VMPFC and PCC, provide top-down influence on both SER and DOP nuclei.

4 | DISCUSSION

In the present study, by combining SGC and a coherence-based phase delay method, we aimed to investigate the temporal organization between DMN regions, thalamus, upper brainstem 5-HT nuclei, and the midbrain DA nuclei. We found that neural activity in the core DMN regions, as measured by the BOLD signal, influences the activity in monoaminergic nuclei in the resting state condition. Thus, refuting our initial hypothesis that 5-HT/DA nuclei provide bottom-up influence on the DMN during resting state.

In line with our previous work (Bär et al., 2016), we observed a positive correlation between DOP and PCC as well as with a large cluster comprising mainly VMPFC, ACC, and midcingulate cortex
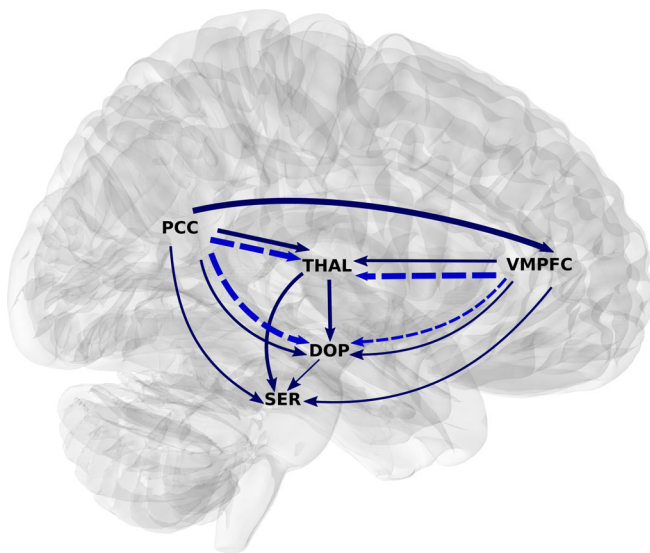
FIGURE 5 Spectral Granger causality (dark blue solid) and significant phase-delay (bright blue dotted). Only stronger SGC between the two ROIs is represented. The width of the lines is proportional to the strength of the metric. The SGC is grossly concordant with phase-delay, that is, the region that Granger cause is that who is also leading in the phase-delay analysis

(MCC). We found similar clusters using SER as seed region, although to a lesser extent.

The strongly significant correlations between DOP/SER neuromodulatory centers with VMPFC, PCC, and ACC/MCC indicates functional integration among these regions (Bär et al., 2016; Hadley et al., 2014). It also agrees with pharmacological studies that explicitly manipulated the plasma concentration of these monoaminergic neurotransmitters to elicit changes in DMN areas (Kunisato et al., 2011; Nagano-Saito et al., 2008). The functional integration between DMN and DOP/SER centers is also supported by anatomical evidence (Azmitia & Segal, 1978; Gaspar, Berger, Febvret, Vigny, & Henry, 1989; Ikemoto, 2007). For example, the DA neurons located in the VTA innervate several DMN areas, including the medial prefrontal cortex, hippocampus, and cingulate cortices (Gaspar et al., 1989; Ikemoto, 2007). Similarly, animal experiments showed that 5-HT-like fibers originating from the DRN and NCS nuclei reach several cortical regions such as the PCC or medial prefrontal areas (Azmitia & Segal, 1978).

We applied spectral GC to functional resting-state data acquired with an ultra-fast fMRI sequence to investigate causal relationships between DOP/SER and core DMN regions. SGC revealed that the top-down direction is the most likely direction of the information flow. Although contrary to our expectation based on reported anatomical findings, the bidirectional SGC approach adopted in this study revealed that SGC values were stronger from cortical areas to DOP/SER than in the opposite direction. From an evolutionary perspective, top-down influences can be seen as the most recent connections in the human brain (Derryberry & Tucker, 1992). It is well-known that during the human evolution of the human brain, new descending connections

were established between the neocortex and the most primitive levels, that is, brainstem and limbic system (Derryberry & Tucker, 1992). An important consequence of the existence of such top-down influences is that cognitive processes mediated by forebrain areas might shape emotional functions of the limbic system and brainstem (Ochsner & Gross, 2008; Phelps & LeDoux, 2005).

Regulation of cortical regions on brainstem structures is also found in the context of the neurovisceral integration model (Thayer & Lane, 2000; Thayer & Lane, 2009). That model posits that frontal areas exert influence on cardiovascular centers located in midbrain/brainstem via limbic structures. This top-down control occurs within a set of functionally connected regions, the so-called central autonomic network, with the main components VMPFC and PCC (Benarroch, 1993). Top-down control is particularly observed when the brain is involved in mental and physical efforts. Such demanding tasks promote cardiovascular responses mediated by brainstem regions, which are, in turn, influenced by the VMPFC (Shoemaker, Norton, Baker, & Luchyshyn, 2015; Wong, Massé, Kimmerly, Menon, & Shoemaker, 2007).

Early experiments in rats and primates revealed the role of the prefrontal cortex in the activation of monoaminergic neurons in the brainstem (Aston-Jones, Chiang, & Alexinsky, 1991; Grahn et al., 1999). For instance, uncontrollable stressors cause excess serotonergic activity in DRN, which produces a broad constellation of behaviors (Grahn et al., 1999). However, when the stressor is controllable, stress-induced activation of the DRN is inhibited by the VMPFC, thus stopping the behavioral sequelae (Amat et al., 2005). Such top-downregulation by the VMPFC over the activity of the DRN is in line with the anatomical evidence that the DRN receives input from infralimbic and prelimbic regions within the VMPFC (Peyron, Petit, Rampon, Jouvet, & Luppi, 1997; Vertes, 2004). Similarly, pharmacological and physiological studies also suggest that the prefrontal cortex tonically modulates subcortical dopaminergic transmission (Jackson, Frost, & Moghaddam, 2001; Karreman & Moghaddam, 1996) mediated through efferent projections to dopaminergic neurons in the VTA (Sesack & Pickel, 1992).

Surprisingly, only a limited number of neuroimaging studies have investigated causal relationships between DMN and midbrain/brainstem areas. Norton and colleagues revealed that during a simple handgrip task, VMPFC exerts a direct influence on serotonergic raphe neurons (Norton, Luchyshyn, & Kevin Shoemaker, 2013). Another recent study using effective connectivity examined alterations within the hippocampal-basal ganglia-SNc/VTA reward circuit in subjects at high risk of psychosis (Winton-Brown et al., 2017). They found reward-induced effective connectivity from the basal ganglia to the SNc/VTA nuclei and that this connectivity is altered in subjects with a high risk of psychosis. This top-down control is not surprising because reward centers project back to dopaminergic cells in the VTA and SNc nuclei (Groenewegen et al., 1991; Zahm & Heimer, 1990; Zahm & Heimer, 1993).

It is also noteworthy to mention that the presence of BOLD-based connectivity, that is, functional or effective, is not necessarily determined by the existence of anatomical connections (Raichle, 2015). The relationship between structural and BOLD-based connectivity cannot be considered as a simple one-to-one mapping (Hawellek,

Hipp, Lewis, Corbetta, & Engel, 2011; O'Reilly et al., 2013). For example, there is evidence that interhemispheric functional connectivity in monkeys is not affected by decreasing structural connectivity (O'Reilly et al., 2013). Similarly, the white matter damage caused by multiple sclerosis in humans has been observed to correlate with increases in functional connectivity (Hawellek et al., 2011). Therefore, it is plausible to suggest, based on our findings that information flows from the core DMN regions to midbrain/brainstem nuclei even if the known anatomical connectivity favors a bottom-up flow.

We further confirmed the top-down influences identified by SGC using a coherence-based approach. Phase-delay (significant values) and SGC showed complementary results in terms of the information flow, that is, the influencing regions in the SGC analysis were those leading in the phase-delay analysis. Interestingly, we found the largest latencies between DMN regions and thalamus. Large latencies can be considered as functionally separated structures, that is, the thalamus seems to be involved in some serial cognitive processing with other areas, for example, executive network, rather than the DMN. This is entirely plausible as the thalamus has been described as part of the executive control network (Bär et al., 2016; Niendam et al., 2012) as well as being functionally interrelated with motor centers of the cerebral cortex (Ansari, Oghabian, & Hossein-Zadeh, 2011).

The agreement between phase-delay and SGC analyses has been repeatedly reported in the literature (Brovelli et al., 2004; Gaglianese et al., 2012; Kayser et al., 2009). Both methods should correlate well in the absence of feedback or reciprocal connection, as demonstrated in simulated and experimental BOLD data (Kayser et al., 2009). However, as discussed earlier, reciprocal connections exist between DMN regions and monoaminergic centers, which can lead to a mismatch in SGC and phase delay results. Thus, the fact that both methods concur may suggest a clear dominance of the descending fibers over the ascending ones at rest.

In this study, the order of the autoregressive model was optimized for each pair of ROIs, resulting in a lag distribution from 0 to 6, with an average value of 3. A large distribution of optimal orders is expected for series with a fast sampling rate because order selection criteria tend to select more complex models in order to capture the dynamics of the interacting time series (Roebroeck et al., 2005). For example, an order of 1 or 2 is generally estimated for a low sampling rate due to the stronger influence of the hemodynamic filtering and temporal down-sampling. We also conducted the SGC analysis by fixing the order to 3, but no appreciable differences were observed. Nonetheless, phase delays and optimal order-lags were comparable. The latencies PCC → DOP = 1.41 s, PCC → THAL = 1.43 s, and VMPFC → THAL = 1.59 s roughly correspond to the mean optimal lag of 1.5 s (3 TR). Finally, it should also be noted that zero order-lag offers no plausible biological justification. However, it might serve as an indicator of potential interactions driven by a third region, where conditional Granger causality could perform better. To keep the model as simple as possible, we did not perform conditional SGC.

It should be recalled that fMRI imaging of the midbrain/brainstem is challenging due to the high susceptibility to signal dropout and geometric distortion. Likewise, the optimization of acquisition parameters must be a compromise between imaging the cortex and lower brain areas (Düzel et al., 2015). Our fMRI parameters were chosen as a trade-off between fMRI imaging of the cortex and brainstem and inference of GC/phase-delay. The 2.5 mm^3 voxel size and 484-ms TR allowed us sufficient spatial and temporal resolution to correctly identify midbrain/brainstem nuclei while reducing confounds on GC and phase-delay estimates.

Along with technical factors like the sampling rate, the nature of the fMRI BOLD signal poses a further challenge for inferring causal relationships. The HRF due to neural activation is sluggish and peaks a few seconds after the onset of neural activity. This characteristic of the HRF implies that even when temporal resolutions in the millisecond range are achieved, it is not possible to distinguish neural events that occur less than 100 ms apart (Hamilton, Chen, Thomason, Schwartz, & Gotlib, 2011). Likewise, the HRF may vary across brain regions and individuals due to non-neuronal processes (Aguirre et al., 1998; Handwerker et al., 2004). Such variations can reverse temporal precedence at the neural level, affecting the inference of both fMRI GC and phase-delay. Indeed, phase-delay values do not represent absolute estimates of neural latencies since the phase-delay method cannot properly distinguish between hemodynamic and neural delays (Sun et al., 2005).

Although these limitations have raised concerns about the reliability/reproducibility of fMRI GC, many experimental and theoretical investigations indicate that GC can be successfully applied to BOLD data, accurately reflecting neuronally-related timing information. Conti et al. found that directed methods such as GC and undirected methods such as conventional Pearson correlation achieve an equivalent degree of intra- and inter-subject variability when used to compute graph-theoretical measures (Conti et al., 2019). In the same vein, Kayser et al. showed that fMRI GC and coherence-based methods produce convergent results, accurately identifying the direction of influence in individuals performing a motor task. Both methods, in agreement with animal and other human studies, detected the leading influence of the supplementary motor area on the posterior parietal cortex (Kayser et al., 2009). Likewise, Wen and colleagues also demonstrated through simulations that fMRI GC correlates strongly with neural GC ($r > .9$) (Wen et al., 2013). These findings speak in favor of fMRI GC's reliability despite the sluggish hemodynamics and low temporal resolution of the BOLD signal.

5 | LIMITATION

In this study, we applied Granger causality and coherence-based phase-delay on resting-state data. Thus, a limitation of the present work is whether findings can be extrapolated to different brain conditions. Even though resting-state fMRI reflects the neuronal baseline activity of the brain (Biswal et al., 1995) and a strong link exists between resting-state and task-based BOLD signals (Cole, Bassett, Power, Braver, & Petersen, 2014; Tavor et al., 2016), it remains a question for future research whether the observed top-down

hierarchical organization persists in the presence of external demands. Indeed, the absence of a task that could validate the resting-state findings is a limitation in this work. It is challenging to find a reliable task that could simultaneously alter the neural activity of DMN areas and monoaminergic nuclei.

The procedure used to define DMN and thalamus ROIs may also be another limitation. For consistency with our previous publications (Bär et al., 2016; de la Cruz et al., 2017; de la Cruz et al., 2019), we opted for using predefined ROIs instead of a data-based methodology, in which ROIs are defined from connectivity or activation peaks (Gaglianese et al., 2012). However, a connectivity-defined ROI methodology would have resulted in higher SCG values and less variability in phase-delay rather than altering the observed top-down directionality according to a simulation study performed by Kayser et al. (2009).

In line with most other studies investigating intra-brain interactions, we chose the bivariate SGC framework to examine causal relationships. However, it is known that the brain shows high interdependence among its regions. This implies that if the two analyzed regions are receiving common input from a third one, it can lead to the appearance of spurious causality in the bivariate SGC. In this context, conditional causality is a suitable approach to handle such cases. However, the application of conditional SGC to partial out the influence of third regions was beyond the scope of the current exploratory study.

6 | CONCLUSION

To the best of our knowledge, this is the first study that aims to investigate causal relationships and relative latencies between core DMN regions and midbrain/brainstem nuclei during resting-state fMRI. We employed an ultra-fast MRI acquisition combined with SGC and phase-delay analyses and found strong consistency between both methods. In contrast to our initial hypothesis that neuromodulatory centers influence BOLD signal fluctuations in the DMN regions and thalamus, the results of the present study indicate a direct influence of DMN regions over monoaminergic centers in midbrain/brainstem.

CONFLICT OF INTERESTS
None of the authors declares any conflict of interest.

AUTHOR CONTRIBUTIONS
Karl-Jürgen Bär and Gerd Wagner conceived the study; Daniel Güllmar and Jürgen R. Reichenbach designed the MRI scan sequences; Andy Schumann and Stefanie Suttkus acquired the data, and Feliberto de la Cruz analyzed the data and wrote the manuscript with input of all authors.

DATA AVAILABILITY STATEMENT
The data that support the findings of this study are available from the corresponding author upon reasonable request.

ORCID
Feliberto de la Cruz https://orcid.org/0000-0002-6529-2679
Andy Schumann https://orcid.org/0000-0002-5691-4325
Karl-Jürgen Bär https://orcid.org/0000-0003-3861-5679

REFERENCES
Abler, B., Roebroeck, A., Goebel, R., Höse, A., Schönfeldt-Lecuona, C., Hole, G., & Walter, H. (2006). Investigating directed influences between activated brain areas in a motor-response task using fMRI. *Magnetic Resonance Imaging*, 24, 181–185. https://doi.org/10.1016/j.mri.2005.10.022

Aguirre, G. K., Zarahn, E., & D'Esposito, M. (1998). The variability of human, BOLD hemodynamic responses. *NeuroImage*, 8, 360–369. https://doi.org/10.1006/nimg.1998.0369

Amat, J., Baratta, M. V., Paul, E., Bland, S. T., Watkins, L. R., & Maier, S. F. (2005). Medial prefrontal cortex determines how stressor controllability affects behavior and dorsal raphe nucleus. *Nature Neuroscience*, 8, 365–371. https://doi.org/10.1038/nn1399

Ansari, A.H.J., Oghabian, M.A., Hossein-Zadeh, G.A., 2011. Assessment of functional and structural connectivity between motor cortex and thalamus using fMRI and DWI, in: 2011 Annual International Conference of the IEEE Engineering in Medicine and Biology Society. pp. 5056–5059. https://doi.org/10.1109/IEMBS.2011.6091252

Ashburner, J. (2007). A fast diffeomorphic image registration algorithm. *NeuroImage*, 38, 95–113. https://doi.org/10.1016/j.neuroimage.2007.07.007

Aston-Jones, G., Chiang, C., & Alexinsky, T. (1991). Discharge of noradrenergic locus coeruleus neurons in behaving rats and monkeys suggests a role in vigilance. *Progress in Brain Research*, 88, 501–520. https://doi.org/10.1016/S0079-6123(08)63830-3

Azmitia, E. C., & Segal, M. (1978). An autoradiographic analysis of the differential ascending projections of the dorsal and median raphe nuclei in the rat. *The Journal of Comparative Neurology*, 179, 641–667. https://doi.org/10.1002/cne.901790311

Bär, K. J., De la Cruz, F., Schumann, A., Koehler, S., Sauer, H., Critchley, H., & Wagner, G. (2016). Functional connectivity and network analysis of midbrain and brainstem nuclei. *NeuroImage*, 134, 53–63. https://doi.org/10.1016/j.neuroimage.2016.03.071

Bär, K. J., Köhler, S., de la Cruz, F., Schumann, A., Zepf, F. D., & Wagner, G. (2020). Functional consequences of acute tryptophan depletion on raphe nuclei connectivity and network organization in healthy women. *NeuroImage*, 207, 116362. https://doi.org/10.1016/j.neuroimage.2019.116362

Barnett, L., & Seth, A. K. (2011). Behaviour of Granger causality under filtering: Theoretical invariance and practical application. *Journal of Neuroscience Methods*, 201, 404–419. https://doi.org/10.1016/j.jneumeth.2011.08.010

Beg, M. F., Miller, M. I., Trouvé, A., & Younes, L. (2005). Computing large deformation metric mappings via geodesic flows of diffeomorphisms. *International Journal of Computer Vision*, 61, 139–157. https://doi.org/10.1023/B:VISI.0000043755.93987.aa

Benarroch, E. E. (1993). The central autonomic network: Functional organization, dysfunction, and perspective. *Mayo Clinic Proceedings*, 68, 988–1001.

Birn, R. M., Smith, M. A., Jones, T. B., & Bandettini, P. A. (2008). The respiration response function: The temporal dynamics of fMRI signal fluctuations related to changes in respiration. *NeuroImage*, 40, 644–654. https://doi.org/10.1016/j.neuroimage.2007.11.059

Biswal, B., Yetkin, F. Z., Haughton, V. M., & Hyde, J. S. (1995). Functional connectivity in the motor cortex of resting human brain using echo-planar MRI. *Magnetic Resonance in Medicine*, 34, 537–541.

Briggs, G. G., & Nebes, R. D. (1975). Patterns of hand preference in a student population. *Cortex*, 11, 230–238.

Brovelli, A., Ding, M., Ledberg, A., Chen, Y., Nakamura, R., & Bressler, S. L. (2004). Beta oscillations in a large-scale sensorimotor cortical network: Directional influences revealed by Granger causality. *Proceedings of the National Academy of Sciences*, *101*, 9849–9854. https://doi.org/10.1073/pnas.0308538101

Buckner, R. L., Andrews-Hanna, J. R., & Schacter, D. L. (2008). The brain's default network. *Annals of the New York Academy of Sciences*, *1124*, 1–38. https://doi.org/10.1196/annals.1440.011

Carhart-Harris, R. L., Leech, R., Erritzoe, D., Williams, T. M., Stone, J. M., Evans, J., ... Nutt, D. J. (2013). Functional connectivity measures after psilocybin inform a novel hypothesis of early psychosis. *Schizophrenia Bulletin*, *39*, 1343–1351. https://doi.org/10.1093/schbul/sbs117

Cole, M. W., Bassett, D. S., Power, J. D., Braver, T. S., & Petersen, S. E. (2014). Intrinsic and task-evoked network architectures of the human brain. *Neuron*, *83*, 238–251. https://doi.org/10.1016/j.neuron.2014.05.014

Conti, A., Duggento, A., Guerrisi, M., Passamonti, L., Indovina, I., & Toschi, N. (2019). Variability and reproducibility of directed and undirected functional MRI connectomes in the human brain. *Entropy*, *21*, 661.

Dahlström, A., & Fuxe, K. (1964). Evidence for the existance of monomaine-containing neurons in the central nervous system. *Acta Physiologica Scandinavica. Supplementum*, *18*, 1–55. https://doi.org/10.1007/BF00160582

de la Cruz, F., Schumann, A., Köhler, S., Bär, K. J., & Wagner, G. (2017). Impact of the heart rate on the shape of the cardiac response function. *NeuroImage*, *162*, 214–225. https://doi.org/10.1016/j.neuroimage.2017.08.076

de la Cruz, F., Schumann, A., Köhler, S., Reichenbach, J. R., Wagner, G., & Bär, K. J. (2019). The relationship between heart rate and functional connectivity of brain regions involved in autonomic control. *NeuroImage*, *196*, 318–328. https://doi.org/10.1016/j.neuroimage.2019.04.014

Derryberry, D., & Tucker, D. M. (1992). Neural mechanisms of emotion. *Journal of Consulting and Clinical Psychology*, *60*, 329–338. https://doi.org/10.1037/0022-006X.60.3.329

Deshpande, G., LaConte, S., James, G. A., Peltier, S., & Hu, X. (2009). Multivariate Granger causality analysis of fMRI data. *Human Brain Mapping*, *30*, 1361–1373. https://doi.org/10.1002/hbm.20606

Diedrichsen, J. (2006). A spatially unbiased atlas template of the human cerebellum. *NeuroImage*, *33*, 127–138. https://doi.org/10.1016/j.neuroimage.2006.05.056

Düzel, E., Guitart-Masip, M., Maass, A., Hämmerer, D., Betts, M. J., Speck, O., ... Kanowski, M. (2015). Midbrain fMRI: Applications, limitations and challenges. In K. Uludag, K. Ugurbil, & L. Berliner (Eds.), *FMRI: From nuclear spins to brain functions* (pp. 581–609). Boston, MA: Springer US. https://doi.org/10.1007/978-1-4899-7591-1_20

Feinberg, D. A., Moeller, S., Smith, S. M., Auerbach, E., Ramanna, S., Glasser, M. F., ... Yacoub, E. (2010). Multiplexed echo planar imaging for sub-second whole brain fmri and fast diffusion imaging. *PLoS One*, *5*, e15710. https://doi.org/10.1371/journal.pone.0015710

Friston, K. J. (1994). Functional and effective connectivity in neuroimaging: A synthesis. *Human Brain Mapping*, *2*, 56–78. https://doi.org/10.1002/hbm.460020107

Gaglianese, A., Costagli, M., Bernardi, G., Ricciardi, E., & Pietrini, P. (2012). Evidence of a direct influence between the thalamus and hMT+ independent of V1 in the human brain as measured by fMRI. *NeuroImage*, *60*, 1440–1447. https://doi.org/10.1016/j.neuroimage.2012.01.093

Gaspar, P., Berger, B., Febvret, A., Vigny, A., & Henry, J. P. (1989). Catecholamine innervation of the human cerebral cortex as revealed by comparative immunohistochemistry of tyrosine hydroxylase and dopamine-beta-hydroxylase. *The Journal of Comparative Neurology*, *279*, 249–271. https://doi.org/10.1002/cne.902790208

Glover, G. H., Li, T. Q., & Ress, D. (2000). Image-based method for retrospective correction of physiological motion effects in fMRI: RETROICOR. *Magnetic Resonance in Medicine*, *44*, 162–167.

Grahn, R., Will, M., Hammack, S., Maswood, S., McQueen, M., Watkins, L., & Maier, S. (1999). Activation of serotonin-immunoreactive cells in the dorsal raphe nucleus in rats exposed to an uncontrollable stressor. *Brain Research*, *826*, 35–43. https://doi.org/10.1016/S0006-8993(99)01208-1

Granger, C. W. J. (1969). Investigating causal relations by econometric models and cross-spectral methods. *Econometrica*, *37*, 424–438. https://doi.org/10.2307/1912791

Greicius, M. D., Krasnow, B., Reiss, A. L., & Menon, V. (2003). Functional connectivity in the resting brain: A network analysis of the default mode hypothesis. *Proceedings of the National Academy of Sciences of the United States of America*, *100*, 253–258. https://doi.org/10.1073/pnas.0135058100

Groenewegen, H. J., Berendse, H. W., Meredith, G. E., Haber, S. N., Voorn, P., Wolters, J. G., & Lohman, A. H. M. (1991). Functional anatomy of the ventral, limbic system innervated striatum. In P. Willner & J. Scheel-Kruger (Eds.), *The mesolimbic dopamine system: From motivation to action* (pp. 19–59). New York: John Wiley and Sons.

Hadley, J. A., Nenert, R., Kraguljac, N. V., Bolding, M. S., White, D. M., Skidmore, F. M., ... Lahti, A. C. (2014). Ventral tegmental area/midbrain functional connectivity and response to antipsychotic medication in schizophrenia. *Neuropsychopharmacology*, *39*, 1020–1030. https://doi.org/10.1038/npp.2013.305

Hamilton, J. P., Chen, G., Thomason, M. E., Schwartz, M. E., & Gotlib, I. H. (2011). Investigating neural primacy in major depressive disorder: Multivariate Granger causality analysis of resting-state fMRI time-series data. *Molecular Psychiatry*, *16*, 763–772. https://doi.org/10.1038/mp.2010.46

Handwerker, D. A., Ollinger, J. M., & D'Esposito, M. (2004). Variation of BOLD hemodynamic responses across subjects and brain regions and their effects on statistical analyses. *NeuroImage*, *21*, 1639–1651. https://doi.org/10.1016/j.neuroimage.2003.11.029

Hawellek, D. J., Hipp, J. F., Lewis, C. M., Corbetta, M., & Engel, A. K. (2011). Increased functional connectivity indicates the severity of cognitive impairment in multiple sclerosis. *Proceedings of the National Academy of Sciences*, *108*, 19066–19071. https://doi.org/10.1073/pnas.1110024108

Hwang, K., Hallquist, M. N., & Luna, B. (2013). The development of hub architecture in the human functional brain network. *Cerebral Cortex*, *23*, 2380–2393. https://doi.org/10.1093/cercor/bhs227

Ikemoto, S. (2007). Dopamine reward circuitry: Two projection systems from the ventral midbrain to the nucleus accumbens–olfactory tubercle complex. *Brain Research Reviews*, *56*, 27–78. https://doi.org/10.1016/j.brainresrev.2007.05.004

Jackson, M. E., Frost, A. S., & Moghaddam, B. (2001). Stimulation of prefrontal cortex at physiologically relevant frequencies inhibits dopamine release in the nucleus accumbens. *Journal of Neurochemistry*, *78*, 920–923. https://doi.org/10.1046/j.1471-4159.2001.00499.x

Jo, H. J., Saad, Z. S., Simmons, W. K., Milbury, L. A., & Cox, R. W. (2010). Mapping sources of correlation in resting state FMRI, with artifact detection and removal. *NeuroImage*, *52*, 571–582. https://doi.org/10.1016/j.neuroimage.2010.04.246

Karreman, M., & Moghaddam, B. (1996). The prefrontal cortex regulates the basal release of dopamine in the limbic striatum: An effect mediated by ventral tegmental area. *The Journal of Neurochemistry*, *66*, 589–598. https://doi.org/10.1046/j.1471

Kayser, A. S., Sun, F. T., & D'Esposito, M. (2009). A comparison of Granger causality and coherency in fMRI-based analysis of the motor system. *Human Brain Mapping*, *30*, 3475–3494. https://doi.org/10.1002/hbm.20771

Kelly, C., de Zubicaray, G., Di Martino, A., Copland, D. A., Reiss, P. T., Klein, D. F., … McMahon, K. (2009). L-Dopa modulates functional connectivity in striatal cognitive and motor networks: A double-blind placebo-controlled study. *The Journal of Neuroscience*, *29*, 7364–7378.

Koot, S., Zoratto, F., Cassano, T., Colangeli, R., Laviola, G., van den Bos, R., & Adriani, W. (2012). Compromised decision-making and increased gambling proneness following dietary serotonin depletion in rats. *Neuropharmacology*, *62*, 1640–1650. https://doi.org/10.1016/j.neuropharm.2011.11.002

Kunisato, Y., Okamoto, Y., Okada, G., Aoyama, S., Demoto, Y., Munakata, A., … Yamawaki, S. (2011). Modulation of default-mode network activity by acute tryptophan depletion is associated with mood change: A resting state functional magnetic resonance imaging study. *Neuroscience Research*, *69*, 129–134. https://doi.org/10.1016/j.neures.2010.11.005

Lauritzen, T. Z., D'Esposito, M., Heeger, D. J., & Silver, M. A. (2009). Top-down flow of visual spatial attention signals from parietal to occipital cortex. *Journal of Vision*, *9*, 1–14. https://doi.org/10.1167/9.13.1

Lin, F. H., Ahveninen, J., Raij, T., Witzel, T., Chu, Y. H., Jääskeläinen, I. P., … Belliveau, J. W. (2014). Increasing fMRI sampling rate improves Granger causality estimates. *PLoS One*, *9*, e100319. https://doi.org/10.1371/journal.pone.0100319

Maldjian, J. A., Laurienti, P. J., & Burdette, J. H. (2004). Precentral gyrus discrepancy in electronic versions of the Talairach atlas. *NeuroImage*, *21*, 450–455.

Maldjian, J. A., Laurienti, P. J., Kraft, R. A., & Burdette, J. H. (2003). An automated method for neuroanatomic and cytoarchitectonic atlas-based interrogation of fMRI data sets. *NeuroImage*, *19*, 1233–1239.

Metzger, C. D., Wiegers, M., Walter, M., Abler, B., & Graf, H. (2016). Local and global resting state activity in the noradrenergic and dopaminergic pathway modulated by Reboxetine and Amisulpride in healthy subjects. *The International Journal of Neuropsychopharmacology*, *19*, pyv080. https://doi.org/10.1093/ijnp/pyv080

Nagano-Saito, A., Leyton, M., Monchi, O., Goldberg, Y. K., He, Y., & Dagher, A. (2008). Dopamine depletion impairs frontostriatal functional connectivity during a set-shifting task. *The Journal of Neuroscience*, *28*, 3697–3706. https://doi.org/10.1523/JNEUROSCI.3921-07.2008

Naidich, T. P., Duvernoy, H. M., Delman, B. N., Sorensen, A. G., Kollias, S. S., & Haacke, E. M. (2009). Gross sectional Anatomy and 3T MRI correlations in axial, coronal and sagittal planes. In *Duvernoy's atlas of the human brain stem and cerebellum: High-field MRI, surface anatomy, internal structure, vascularization and 3 D Sectional Anatomy* (p. 561–835). Vienna: Springer-Verlag Wien. https://doi.org/10.1007/978-3-211-73971-6_13

Niendam, T. A., Laird, A. R., Ray, K. L., Dean, Y. M., Glahn, D. C., & Carter, C. S. (2012). Meta-analytic evidence for a superordinate cognitive control network subserving diverse executive functions. *Cognitive, Affective, & Behavioral Neuroscience*, *12*, 241–268. https://doi.org/10.3758/s13415-011-0083-5

Norton, K. N., Luchyshyn, T. A., & Kevin Shoemaker, J. (2013). Evidence for a medial prefrontal cortex–hippocampal axis associated with heart rate control in conscious humans. *Brain Research*, *1538*, 104–115. https://doi.org/10.1016/j.brainres.2013.09.032

Ochsner, K. N., & Gross, J. J. (2008). Cognitive emotion regulation. *Current Directions in Psychological Science*, *17*, 153–158. https://doi.org/10.1111/j.1467-8721.2008.00566.x

O'Reilly, J. X., Croxson, P. L., Jbabdi, S., Sallet, J., Noonan, M. P., Mars, R. B., … Baxter, M. G. (2013). Causal effect of disconnection lesions on interhemispheric functional connectivity in rhesus monkeys. *Proceedings of the National Academy of Sciences*, *110*, 13982–13987. https://doi.org/10.1073/pnas.1305062110

Paxinos, G., & Huang, X.-F. (1995). *Atlas of the human brainstem*, San Diego, CA: Academic Press.

Peyron, C., Petit, J.-M., Rampon, C., Jouvet, M., & Luppi, P.-H. (1997). Forebrain afferents to the rat dorsal raphe nucleus demonstrated by retrograde and anterograde tracing methods. *Neuroscience*, *82*, 443–468. https://doi.org/10.1016/S0306-4522(97)00268-6

Phelps, E. A., & LeDoux, J. E. (2005). Contributions of the amygdala to emotion processing: From animal models to human behavior. *Neuron*, *48*, 175–187. https://doi.org/10.1016/J.NEURON.2005.09.025

Raichle, M. E. (2015). The restless brain: How intrinsic activity organizes brain function. *Philosophical Transactions of the Royal Society of London. Series B, Biological Sciences*, *370*, 20140172. https://doi.org/10.1098/rstb.2014.0172

Raichle, M. E., MacLeod, A. M., Snyder, A. Z., Powers, W. J., Gusnard, D. A., & Shulman, G. L. (2001). A default mode of brain function. *Proceedings of the National Academy of Sciences*, *98*, 676–682. https://doi.org/10.1073/pnas.98.2.676

Roebroeck, A., Formisano, E., & Goebel, R. (2005). Mapping directed influence over the brain using Granger causality and fMRI. *NeuroImage*, *25*, 230–242. https://doi.org/10.1016/j.neuroimage.2004.11.017

Roebroeck, A., Formisano, E., & Goebel, R. (2011). The identification of interacting networks in the brain using fMRI: Model selection, causality and deconvolution. *NeuroImage*, *58*, 296–302. https://doi.org/10.1016/j.neuroimage.2009.09.036

Rolland, B., Amad, A., Poulet, E., Bordet, R., Vignaud, A., Bation, R., … Jardri, R. (2015). Resting-state functional connectivity of the nucleus accumbens in auditory and visual hallucinations in schizophrenia. *Schizophrenia Bulletin*, *41*, 291–299. https://doi.org/10.1093/schbul/sbu097

Schumann, A., Köhler, S., de la Cruz, F., Güllmar, D., Reichenbach, J. R., Wagner, G., & Bär, K.-J. (2018). The use of physiological signals in brainstem/midbrain fMRI. *Frontiers in Neuroscience*, *12*, 718. https://doi.org/10.3389/fnins.2018.00718

Schwarz, G. (1978). Estimating the dimension of a model. *The Annals of Statistics*, *6*, 461–464. https://doi.org/10.1214/aos/1176344136

Sesack, S. R., & Pickel, V. M. (1992). Prefrontal cortical efferents in the rat synapse on unlabeled neuronal targets of catecholamine terminals in the nucleus accumbens septi and on dopamine neurons in the ventral tegmental area. *The Journal of Comparative Neurology*, *320*, 145–160. https://doi.org/10.1002/cne.903200202

Seth, A. K., Chorley, P., & Barnett, L. C. (2013). Granger causality analysis of fMRI BOLD signals is invariant to hemodynamic convolution but not downsampling. *NeuroImage*, *65*, 540–555. https://doi.org/10.1016/j.neuroimage.2012.09.049

Sheehan, D. V., Lecrubier, Y., Sheehan, K. H., Amorim, P., Janavs, J., Weiller, E., … Dunbar, G. C. (1998). The mini-international neuropsychiatric interview (M.I.N.I.): The development and validation of a structured diagnostic psychiatric interview for DSM-IV and ICD-10. *The Journal of Clinical Psychiatry*, *59*(Suppl 2), 22–57.

Sherman, S. M. (2007). The thalamus is more than just a relay. *Current Opinion in Neurobiology*, *17*, 417–422. https://doi.org/10.1016/j.conb.2007.07.003

Shoemaker, J. K., Norton, K. N., Baker, J., & Luchyshyn, T. (2015). Forebrain organization for autonomic cardiovascular control. *Autonomic Neuroscience: Basic & Clinical*, *188*, 5–9. https://doi.org/10.1016/j.autneu.2014.10.022

Stenner, M.-P., Litvak, V., Rutledge, R. B., Zaehle, T., Schmitt, F. C., Voges, J., … Dolan, R. J. (2015). Cortical drive of low-frequency oscillations in the human nucleus accumbens during action selection. *Journal of Neurophysiology*, *114*, 29–39. https://doi.org/10.1152/jn.00988.2014

Sun, F. T., Miller, L. M., & D'Esposito, M. (2005). Measuring temporal dynamics of functional networks using phase spectrum of fMRI data. *NeuroImage*, *28*, 227–237. https://doi.org/10.1016/j.neuroimage.2005.05.043

Tavor, I., Parker Jones, O., Mars, R. B., Smith, S. M., Behrens, T. E., & Jbabdi, S. (2016). Task-free MRI predicts individual differences in brain

activity during task performance. *Science (80-)*, *352*, 216–220. https://doi.org/10.1126/science.aad8127

Thayer, J. F., & Lane, R. D. (2000). A model of neurovisceral integration in emotion regulation and dysregulation. *Journal of Affective Disorders*, *61*, 201–216. https://doi.org/10.1016/S0165-0327(00)00338-4

Thayer, J. F., & Lane, R. D. (2009). Claude Bernard and the heart-brain connection: Further elaboration of a model of neurovisceral integration. *Neuroscience and Biobehavioral Reviews*, *33*, 81–88. https://doi.org/10.1016/j.neubiorev.2008.08.004

Tomasi, D., & Volkow, N. D. (2014). Functional connectivity of substantia nigra and ventral tegmental area: Maturation during adolescence and effects of ADHD. *Cerebral Cortex*, *24*, 935–944. https://doi.org/10.1093/cercor/bhs382

Ungerstedt, U. (1971). Stereotaxic mapping of the monoamine pathways in the rat brain. *Acta Physiologica Scandinavica*, *367*, 1–48. https://doi.org/10.1111/j.1365-201x.1971.tb10998.x.

van de Ven, V., Wingen, M., Kuypers, K. P. C., Ramaekers, J. G., & Formisano, E. (2013). Escitalopram decreases cross-regional functional connectivity within the default-mode network. *PLoS One*, *8*, e68355. https://doi.org/10.1371/journal.pone.0068355

van Wingen, G. A., Tendolkar, I., Urner, M., van Marle, H. J., Denys, D., Verkes, R.-J., & Fernández, G. (2014). Short-term antidepressant administration reduces default mode and task-positive network connectivity in healthy individuals during rest. *NeuroImage*, *88*, 47–53. https://doi.org/10.1016/j.neuroimage.2013.11.022

Vertes, R. P. (2004). Differential projections of the infralimbic and prelimbic cortex in the rat. *Synapse*, *51*, 32–58. https://doi.org/10.1002/syn.10279

Wagner, G., de la Cruz, F., Köhler, S., Bär, K.-J., Köhler, S., & Bär, K.-J. (2017). Treatment associated changes of functional connectivity of midbrain/brainstem nuclei in major depressive disorder. *Scientific Reports*, *7*, 8675. https://doi.org/10.1038/s41598-017-09077-5

Wagner, G., Krause-Utz, A., de la Cruz, F., Schumann, A., Schmahl, C., & Bär, K.-J. (2018). Resting-state functional connectivity of neurotransmitter producing sites in female patients with borderline personality disorder. *Progress in Neuro-Psychopharmacology & Biological Psychiatry*, *83*, 118–126. https://doi.org/10.1016/j.pnpbp.2018.01.009

Welch, P. (1967). The use of fast Fourier transform for the estimation of power spectra: A method based on time averaging over short, modified periodograms. *IEEE Transactions on Audio and Electroacoustics*, *15*, 70–73. https://doi.org/10.1109/TAU.1967.1161901

Wen, X., Rangarajan, G., & Ding, M. (2013). Is Granger causality a viable technique for analyzing fMRI data? *PLoS One*, *8*, e67428. https://doi.org/10.1371/journal.pone.0067428

Winton-Brown, T., Schmidt, A., Roiser, J. P., Howes, O. D., Egerton, A., Fusar-Poli, P., ... McGuire, P. (2017). Altered activation and connectivity in a hippocampal–basal ganglia–midbrain circuit during salience processing in subjects at ultra high risk for psychosis. *Translational Psychiatry*, *7*, e1245. https://doi.org/10.1038/tp.2017.174

Wong, S. W., Massé, N., Kimmerly, D. S., Menon, R. S., & Shoemaker, J. K. (2007). Ventral medial prefrontal cortex and cardiovagal control in conscious humans. *NeuroImage*, *35*, 698–708. https://doi.org/10.1016/J.NEUROIMAGE.2006.12.027

Yelnik, J., François, C., Percheron, G., & Heyner, S. (1987). Golgi study of the primate substantia nigra. I. Quantitative morphology and typology of nigral neurons. *The Journal of Comparative Neurology*, *265*, 455–472. https://doi.org/10.1002/cne.902650402

Zahm, D. S., & Heimer, L. (1990). Two transpallidal pathways originating in the rat nucleus accumbens. *The Journal of Comparative Neurology*, *302*, 437–446. https://doi.org/10.1002/cne.903020302

Zahm, D. S., & Heimer, L. (1993). Specificity in the efferent projections of the nucleus accumbens in the rat: Comparison of the rostral pole projection patterns with those of the core and shell. *The Journal of Comparative Neurology*, *327*, 220–232. https://doi.org/10.1002/cne.903270205